Evaluating the Effects of Precipitation and Evapotranspiration on Soil Moisture Variability Within CMIP5 Using SMAP and ERA5 Data

Xuan Xi[1] [ID], Qianlai Zhuang[1,2] [ID], Seungbum Kim[3] [ID], and Pierre Gentine[4] [ID]

[1]Department of Earth, Atmospheric, and Planetary Sciences, Purdue University, West Lafayette, IN, USA, [2]Department of Agronomy, Purdue University, West Lafayette, IN, USA, [3]NASA Jet Propulsion Laboratory, Pasadena, CA, USA, [4]Department of Earth of Environmental Engineering, Columbia University, New York, NY, USA

Abstract The effects of precipitation (Pr) and evapotranspiration (ET) on surface soil moisture (SSM) play an essential role in the land-atmosphere system. Here we evaluate multimodel differences of these effects within the Coupled Model Intercomparison Project Phase 5 (CMIP5) compared to Soil Moisture Active Passive (SMAP) products and ECMWF Reanalysis v5 (ERA5) as references in a frequency domain. The variability of SSM, Pr, and ET within three frequency bands ($1/7 \sim 1/30$ days^{-1}, $1/30 \sim 1/90$ days^{-1}, and $1/90 \sim 1/365$ days^{-1}) after normalization is quantified using Fourier transform. We analyze the impact of ET and Pr on SSM variability based on a transfer function assuming that these variables form a linear time-invariant (LTI) system. For the total effects of ET and Pr on SSM variability, the CMIP5 estimations are smaller than the reference data in the two higher frequency bands and are larger than the reference data in the lowest frequency band. Besides, the effects on SSM by Pr and ET are found to be different across the three frequency bands. In each frequency band, the variability of the factor that dominates SSM (i.e., Pr or ET) from CMIP5 is smaller than that from the references. This study identifies the spatiotemporal distribution of differences between CMIP5 models and references (SMAP and ERA5) in simulating ET and Pr effects on SSM within three frequency bands. This study provides insightful information on how soil moisture variability is affected by varying precipitation and evapotranspiration at different time scales within Earth System Models.

Plain Language Summary Climate is influenced by the interactions between the land surface and atmosphere boundary, and soil moisture is a key component of these physical processes. Precipitation and evapotranspiration, as two major variables involved in these interactions, have been largely regarded as essential processes affecting soil moisture dynamics. However, Earth System Models have large uncertainties in simulating these effects. This study compares the average performance of 14 Earth System Models in capturing the effects of precipitation and evapotranspiration on surface soil moisture variability. We find that (a) soil moisture is mainly affected by precipitation at weekly to seasonal time scales and by evapotranspiration at seasonal to annual time scales; (b) compared to two largely used reference data, the total effects of precipitation and evapotranspiration on soil moisture is smaller at weekly to seasonal time scales and are larger at seasonal to annual time scale; and (c) spatially, models tend to simulate less variability of precipitation or evapotranspiration as a major control on surface soil moisture.

1. Introduction

As one of the essential states in the Earth system, soil moisture plays an important role in land-atmosphere interactions (Green et al., 2019; Koster et al., 2004; Seneviratne et al., 2006, 2010). The exploration and quantification of land-atmosphere interactions is important for Earth system study and climate-change projections (Santanello et al., 2018; Seneviratne et al., 2010; Suni et al., 2015). The spatial and temporal dynamics of soil moisture (SM) depend on the variability of multiple hydrological processes, such as precipitation, interception, evapotranspiration, runoff, and drainage (Bonan, 1996; Famiglietti & Rodell, 2013; McCabe & Wolock, 2013). Since these processes are complex and show large heterogeneity spatiotemporally, it is hard to quantify all of their resulting impacts on soil moisture. We focus here on the two largest terrestrial water fluxes that are highly related to soil moisture variability: precipitation (Pr), which is the primary water source of soil moisture and also one of the atmospheric forcing variables for land surface processes, and evapotranspiration (ET), which is a primary water cycling process affecting soil moisture.

Previously, the couplings between SM, Pr, and ET variability have been studied using SM temporal autocorrelation. Assuming that SM dynamics as being forced by a random precipitation time series (i.e., white noise) and damped by an exponential damping term related to evapotranspiration losses, the temporal variability of SM can be reasonably approximated by a first-order Markov process, which results in the SM time series exhibiting a red noise spectrum (Delworth & Manabe, 1988). Based on this, many studies have attempted to characterize these effects within a time-frequency domain. Wu et al. (2002) showed that the response of SM to Pr at long time scales could be identified by its phase shifting and amplitude damping. The relationship between SM and Pr spectra was further explored using the integral time scale to show that SM spectra decays more rapidly than a red noise due to Pr departing from white noise at high frequency, and the damping term of ET losses was found to be bounded by the maximum of ET (Katul et al., 2007). Similarly, the integral time scale was used to reveal the dynamics of SM memory and its correlation with Pr and ET (Ghannam et al., 2016). Based on previous studies (Katul et al., 2007), the SM spectrum was found that could not be explained solely by precipitation effects on longer time scales (Nakai et al., 2014). By performing this kind of spectral analysis on a regional scale, Pr was found to be the main but not the only factor affecting SM variability (Zhou et al., 2020).

Although the coupling between SM, Pr, and ET has been intensively studied, how Earth System Models (ESMs) perform in capturing the effects of Pr and ET on SM variability globally and at different time scales is still not completely understood. There are two major challenges. One is the lack of sufficient accurate in-situ soil moisture measurements at the global scale. Because of this, previous studies have been limited to the use of in situ soil moisture observations to investigate its correlations with Pr and ET in limited regions (e.g., Ford et al., 2015; Wu et al., 2002). Recently, advanced remote sensing technology, such as NASA's Soil Moisture Active Passive (SMAP) mission (Entekhabi et al., 2010), provides global retrievals of surface soil moisture (top ~5 cm of the soil column) that can be used to constrain land-atmosphere interaction observations over different spatiotemporal scales. SMAP soil moisture products match well with in situ SSM observations by showing high accuracy that meets its accuracy requirement (unbiased root-mean-square error < 0.04 m^3/m^3) (Chan et al., 2016, 2018; Colliander et al., 2017, 2021). In addition, SMAP surface soil moisture retrievals show higher accuracy measured by a global average anomaly correlation over the majority of available land pixels compared to Soil Moisture Ocean Salinity (SMOS) and Advanced SCATterometer (ASCAT) (Chen et al., 2018). With the SMAP SSM measurements, the analysis of the Pr and ET effects on SSM can be conducted on a near-global basis rather than being limited by the sparse network of soil moisture observations.

Another challenge is that, due to the complexity and the large number of processes involved in land-atmosphere interactions, the representation of couplings between SM, Pr, and ET highly relies on parameterizations within ESMs, which leads to large uncertainties in identifying the effects of Pr and ET on SM variability (Seneviratne et al., 2010). In addition, the effects of Pr and ET on SM are mostly identified based on correlation analysis in the time domain (Feng & Liu, 2015; Guo et al., 2006; Sehler et al., 2019; Wang et al., 2021). For the time-domain approach, although we can know about the correlation strength between Pr or ET and SM, how the effects of Pr and ET on SM perform across different time scales is still ambiguous. The transfer function (Haykin & Van Veen, 2007), as a mathematical representation of the differential equation of system dynamics, can be used to address this kind of problem using frequency domain analysis. Assuming a linear time-invariant (LTI) system (Phillips et al., 2003), the transfer function can be developed to describe the relationship between the signal input and response without considering its specific structure and parameters. Therefore, it can be used to investigate the effects of Pr and ET on SM across different time scales in the frequency domain, assuming they are an LTI system. Spectral analysis based on the LTI system has been applied to other hydrological research like the runoff-storage relationship (Riegger & Tourian, 2014) and the surface flow in the river during floods (Bailly-Comte et al., 2008).

The fifth phase of the Coupled Model Intercomparison Project (CMIP5; Taylor et al., 2012) integrates a set of model experiments to improve our knowledge of climate change and climate variability and provides an opportunity for the multimodel assessment of land-atmospheric processes and variability. Evaluation of CMIP5 has been an ongoing interest in the research community (Yuan et al., 2021). Although evaluations of land-atmosphere interactions related to soil moisture within CMIP5 have been performed earlier (e.g., Berg & Sheffield, 2018; Dirmeyer et al., 2013; Levine et al., 2016), few studies have characterized the temporal behavior of SM globally in order to illustrate the model performance. Therefore, this study takes advantage of the CMIP5 intercomparison project to evaluate 14 ESMs with regard to the effects of Pr and ET on SSM variability.

We aim to address two main questions: (a) how do the effects of Pr and ET on SSM variability change across time scales? And (b) how do the ESMs within CMIP5 perform in capturing these effects? Specifically, these effects are analyzed within three frequency bands: (a) weekly to monthly time scales ($1/7 \sim 1/30$ days^{-1}), (b) monthly to seasonal time scales ($1/30 \sim 1/90$ days^{-1}), and (c) seasonal to annual time scales ($1/90 \sim 1/365$ days^{-1}) at the global scale. First, a Fourier analysis (Thomson & Emery, 2014; Wilks, 2011) is conducted to determine the variability and power spectra of SSM, Pr, and ET by decomposing their time series into the three frequency bands. Then, we built an LTI system and characterized the effects of Pr and ET on SSM from a multi-frequency perspective based on its transfer function. We further identified these effects by evaluating the relationships between the spectral slopes of the three variables. All analysis is conducted at the same spatial resolution ($\sim$36 km^2) as the SMAP product (specifically, Level 3 Radiometer Global Daily 36 km EASE-Grid Soil Moisture, Version 7) provided.

In Section 2, we first describe the models and data used. Then, we detail our methodology for spectral analysis. In the first part of Section 3, we show the results to be compared with CMIP5 simulations as the reference. In the second part, we perform comparative analyses to evaluate the multimodel differences within CMIP5 compared to the reference. In the third part, we investigate uncertainties that may exist in this study. Finally, in Section 4, we summarize our findings and discuss the impacts of the research.

2. Methods

2.1. Overview

In this section, we first describe the data collection within CMIP5, SMAP observation data, and ERA5 reanalysis data. Second, we detail the methodology from the data preprocessing to the final multimodel comparison. Specifically, Section 2.3 describes the preprocessing of SMAP products and CMIP5 simulations. Section 2.4 describes the processes to get the power spectra used for further analysis. Next, Section 2.5 defines the normalized variability of SSM, Pr, and ET and introduces the approach for investigating the effects of Pr and ET on SSM based on the normalized variability. Section 2.6 describes the spectral slopes of SSM, Pr, and ET time series and how to summarize their auto-correlation characteristics. Figure 1 summarizes the steps described in Sections 2.4, 2.5, and 2.6. Finally, Section 2.7 describes the comparison between CMIP5 simulations and the two reference datasets (i.e., SMAP and ERA5).

2.2. Data Organizing

2.2.1. CMIP5 Models

The CMIP5 project conducted a set of model experiments to improve our knowledge of climate variability from past to present and into the future (Taylor et al., 2012). Here we use the daily simulations of 14 ESMs from the historical experiment within CMIP5. The models are selected based on the availability of daily outputs required for the spectral analysis within the same temporal coverage from 01/01/1950 to 12/31/2005 (Table S1 in the Supporting Information S1). To evaluate the effects of Pr and ET (i.e., atmospheric water supply and loss) on SSM variability, we analyze the simulated SSM (top 10 cm), Pr, and ET (variable mrsos, pr, and hfls in the CMIP5 archive, respectively). We use only one ensemble member—"r1i1p1" (where *r* for realization, *i* for initialization, and *p* for physics).

2.2.2. Reference Data

2.2.2.1. SMAP Soil Moisture Data

The NASA SMAP satellite was launched in January 2015 and has been measuring SSM (moisture in the top $\sim$5 cm of the soil column) globally every 2$\sim$3 days (Entekhabi et al., 2010). In this study, we use its Level 3 Radiometer Global Daily 36 km EASE-Grid Soil Moisture, Version 7 (O'Neill et al., 2020) with the retrievals from both 6 a.m. descending passes and 6 p.m. ascending passes. Although its 6 p.m. retrievals show more degradation than its 6 a.m. retrievals due to the required vertical thermal equilibrium assumption in its algorithm, this degradation has been shown to be small (Chan et al., 2018; O'Neill et al., 2018). Therefore, we use both retrievals to best use the observational information. The SMAP Level 3 product was developed based on geophysical parameters derived from its Level 1 and Level 2 products. It was spatiotemporally re-sampled to the global cylindrical
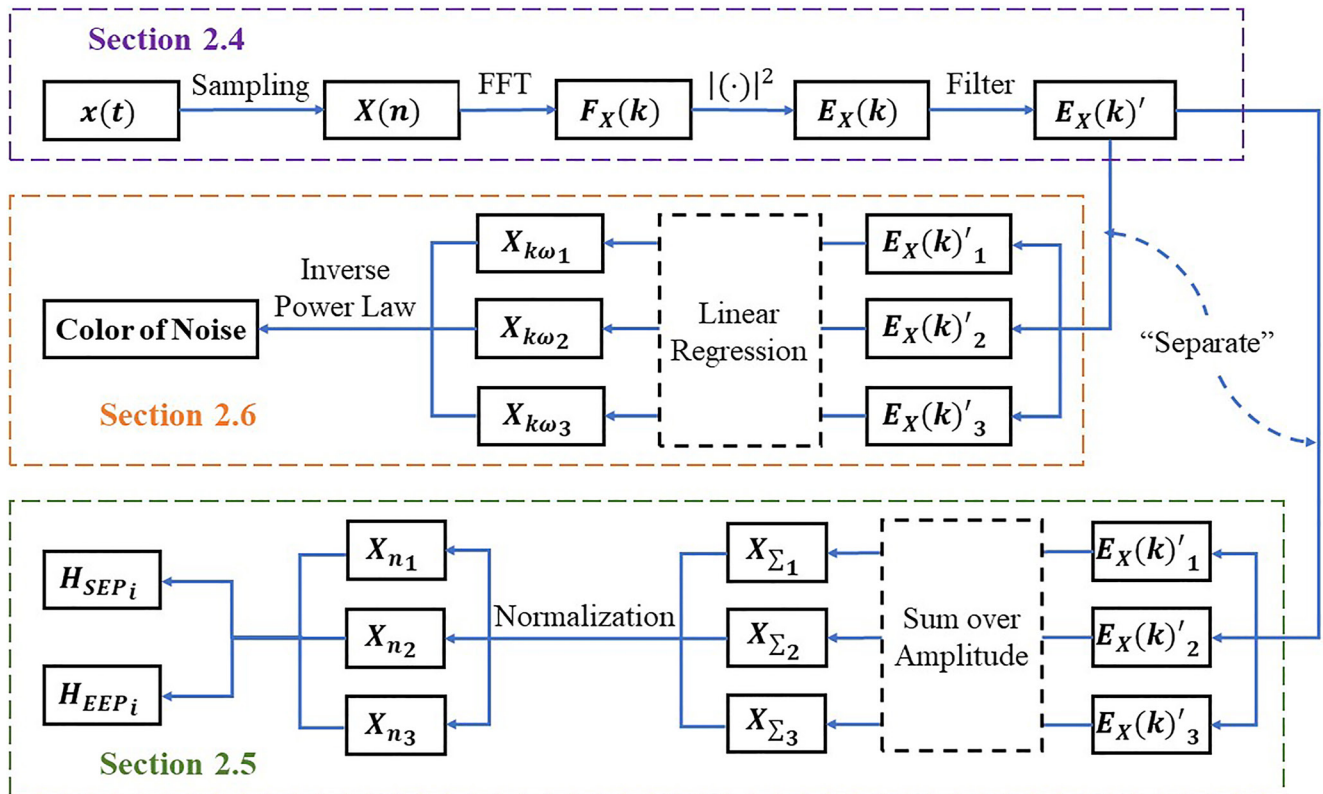
Figure 1. Overview of the data processing. The purple, green, and orange dashed boxes are steps for Sections 2.4, 2.5, and 2.6, respectively. X represents surface soil moisture, precipitation, and evapotranspiration, since the procedures to deal with their time series (i.e., $x(t)$) are the same. The number "1," "2," and "3" (hereafter being referred as i) represent three frequency bands in the order of weekly to monthly (7 ~ 30 days), monthly to seasonal (30 ~ 90 days), and seasonal to annual (90 ~ 365 days) time scales. $x(n)$ is the discrete series sampled from $x(t)$. $F_X(k)$ is the amplitude spectrum of X from $x(n)$ using the Fast Fourier Transform (FFT). $E_X(k)$ is the power spectrum of X as the square of the absolute value of its amplitude. $E_X(k)'$ is the filtered $E_X(k)$ to the frequency band within 7–365 days. $E_X(k)'_i$ is $E_X(k)'$ being "separated" into three frequency bands: weekly to monthly ($i = 1$), monthly to seasonal ($i = 2$), and seasonal to annual ($i = 3$). The sum of spectral amplitudes of X (X_{Σ_i}) and the spectral slopes of X (X_{kw_i}) is gotten from $E_X(k)'_i$ based on "sum over amplitude" and "linear regression" within the ith frequency band, respectively. In the green dashed box, X_{n_i} is gotten from X_{Σ_i} based on normalization across the three frequency bands, and then H_{SEP_i} and H_{EEP_i} are two ratios used to analyze the effects of Pr and ET on SSM defined in Section 2.5. In the orange dashed box, X_{kw_i} are presented as the colors of noise defined in Section 2.6.

EASE-Grid 2.0 to make each grid cell has a nominal size of approximately 36×36 km^2 regardless of longitude and latitude (Brodzik et al., 2012).

In addition, SMAP SSM retrievals have been shown to exhibit potential errors in heavily vegetated areas, frozen soils, and regions with the presence of water bodies (Entekhabi et al., 2014; McColl et al., 2017; Wrona et al., 2017). Therefore, we masked SSM retrievals in regions identified as dense vegetation cover (vegetation water content >5 kg/m^2), frozen landscapes (surface temperature < 0°C), and the presence of water bodies (water body fraction >5% coverage of a pixel), which is similar to a previous study (McColl et al., 2017).

2.2.2.2. ERA5 Precipitation and Evapotranspiration Data

The reference Pr and ET data are collected from ERA5 (Hersbach et al., 2018), which is the fifth-generation reanalysis of ECMWF (European Centre for Medium-Range Weather Forecasts) as the next generation of representative satellite-observational data. ERA5 reanalysis is achieved by data assimilation, which combines weather forecasts with observations in an optimal way every few hours to produce the best estimate of the state of the atmosphere. In this way, ERA5 combines model data and observations into a globally complete and consistent data set. Large efforts have been made on evaluating both precipitation (Jiao et al., 2021; Rivoire et al., 2021; Tarek et al., 2020) and evapotranspiration (Martens et al., 2020; Pelosi & Chirico, 2021; Pelosi et al., 2020) from ERA5 reanalysis against multi-source of observations on regional and global scales. Although this reanalysis data cannot be fully regarded as observations due to more incomprehensible errors and uncertainties associated with its model-dependent nature (Parker, 2016), these extensive evaluations have demonstrated that ERA5 reanalysis

data can serve as good proxies for observations in modeling and assessment of hydrological processes. In this study, we use "total precipitation" (units: m) and "evaporation" (units: m of water equivalent) estimates as references of Pr and ET, respectively, to compare with CMIP5 simulations on a global scale. This ERA5 data set has a spatial resolution of $0.25° \times 0.25°$ for the atmosphere at an hourly temporal resolution. We collect the ERA5 hourly data within the same temporal coverage as SMAP, spanning 1 April 2015–31 December 2020. Then we convert them into UTC-day total precipitation and evapotranspiration (units: m) based on (Hersbach et al., 2018):

$$\text{Pr}_d = \sum_{hr=1}^{23} \text{Pr}_{hr} + \text{Pr}_{d+1\,00UTC} \tag{1}$$

$$\text{ET}_d = \sum_{hr=1}^{23} \text{ET}_{hr} + \text{ET}_{d+1\,00UTC} \tag{2}$$

where hr is hour and d is the day of interest ($d + 1$ is the next day). In this way, we get daily precipitation and evapotranspiration time series (i.e., Pr_d and ET_d) for further analysis. We also use the same subset of ERA5 datasets and the same method to collect daily potential evaporation (PE) (units: m) with the same temporal coverage for comparison with ET.

2.3. Data Preprocessing

First, since the SMAP SSM retrievals are temporally discontinuous on a daily time scale, we perform a gap-filling to make it a daily data set. Specifically, we first use a long-term global daily soil moisture data set derived from AMSR-E and AMSR2 (named as NNsm; Yao & Lu, 2020) to fill part of the missing values in SMAP SSM retrievals. Then we fill in the remaining missing values using the moving average. Next, for those time series that still have gaps longer than the length of the moving window, we fill the gaps with estimates inferred from forward and reverse autoregressive fits to the samples by using autoregressive modeling. The choices of the parameters during this gap-filling process are decided by the corresponding uncertainty analysis, which will be discussed in detail in Section 3.3. To validate the gap-filled SMAP SSM data, we use in-situ SSM data from 16 sites within the International Soil Moisture Network (ISMN; Dorigo et al., 2011, 2013). We select these sites based on 11 vegetation types and five latitude bands, which are both commonly-used ways to categorize the land surface globally (Xi et al., 2022). The statistical errors between gap-filled results and in-situ observations are close to or even better than that between original SMAP retrievals and in-situ observations within ISMN (Tables S2 and S3 in the Supporting Information S1), indicating our gap-filled SMAP data are valid for further analysis.

In addition, the CMIP5 simulations used in this study span decades. Therefore, some regions may show long-term secular trends. To avoid such long-term trends introducing errors into the power spectrum when performing Fourier analysis next, we removed these trends by subtracting an optimal (least squares) fitted linear regression from the original data so that the time series after detrending has a mean value of zero. Thus, we can focus on the intra-annual fluctuations of the time series.

2.4. Obtaining Power Spectra From Time Series

In this study, we perform the variability analysis from two aspects: one is the ratio of the normalized variability, and another is the spectral slope that can be indicated as colors of noise. Both require further steps based on obtaining the power spectra of SSM, Pr, and ET. Since the steps to get the power spectra of the three variables are the same, here we use X to represent SSM, Pr, or ET. There are four steps to get the filtered power spectra of X.

Starting from the top-left corner of Figure 1, $x(n)$, as the data obtained from either CMIP5, SMAP, or ERA5, are the discrete series sampled from $x(t)$ based on the sampling number (N) (i.e., the number of days). Next, we get the amplitude spectrum of X ($F_X(k)$) from $x(n)$ based on the Fast Fourier Transform (FFT), a faster algorithm for the Discrete Fourier Transform (DFT). Both approaches decompose the time series into orthogonal sinusoidal frequency components so that the variability within each component can be investigated separately. In this way, the oscillations of time series ($x(t)$) can be identified through the spectra in the frequency domain.

Then we get the power spectrum of X from its amplitude spectrum as $E_X(k) = |F_X(k)|^2$. We only keep $E_X(k)$ with the frequency ranging from $1/2$ to $1/N$ day^{-1} since the spectrum is symmetrical about the Nyquist frequency ($f_s/2$, where f_s is sampling frequency). For all time-series data, we use 1 day^{-1} as the sampling frequency from
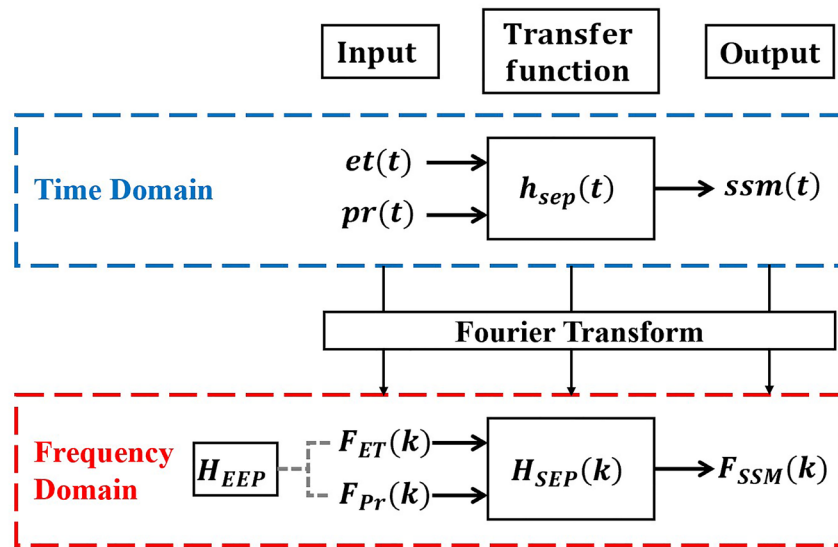
Figure 2. Diagram of the conceptual linear time-invariant (LTI) system with the excitations as et(t) and $pr(t)$, the response as ssm(t), and the transfer function as $h_{sep}(t)$ in the time domain. The form in the time domain is shown in the blue box. By performing Fourier transform, the corresponding form of the LTI system in the frequency domain is shown in the red box, where $F_{ET}(k)$, $F_{Pr}(k)$, and $F_{SSM}(k)$ is the Fourier transform (amplitude spectrum) of et(t), $pr(t)$, and ssm(t), and $H_{SEP}(k)$ is the Fourier transform of the transfer function $h_{sep}(t)$. H_{EEP} is the fraction of ET variability to the sum of ET and Pr variability in the frequency domain.

$x(t)$ to $F_X(k)$ since they are all available at a daily interval. The frequency for each sample is based on its normalized frequency and frequency resolution.

The last step is to restrict our investigation within a weekly to annual frequency band (i.e., 1/7 days^{-1} ∼ 1/365 days^{-1}). There are two reasons to remove frequencies larger than 1/7 days^{-1}: (a) the gap-filling process for SMAP retrievals may introduce high-frequency variability as noise; (b) the random error in the remotely sensed SSM (e.g., SMAP retrievals) could spuriously inflate the high-frequency portion of the SSM spectra, especially on time scales smaller than 3 days (Su et al., 2014). These spuriously inflated high-frequency noises are usually absent from CMIP5 models. The reason to remove frequencies smaller than 1/365 days^{-1} is that, compared to CMIP5 models with multi-decade records, the temporal coverage of SMAP retrievals is too short to support an inter-annual analysis. To achieve this restriction, we filter all time series with a low-pass filter and a high-pass filter with the cutoff frequency as 1/7 days^{-1} and 1/365 days^{-1}, respectively. In this way, we get $E_X(k)'$ as the filtered spectra with frequencies within 1/7 days^{-1} to 1/365 days^{-1} from $E_X(k)$.

2.5. Analysis of the Effects of Pr and ET on SSM Variability

Both Pr and ET affect SSM variability. Pr is the dominant water source of SSM, while ET is the major loss term affecting SSM loss in most climates. Thus, increasing Pr will increase SSM, and increasing ET will decrease SSM (without considering the saturation condition).

Here we aim to examine the effects of ET and Pr on SSM variability within the three frequency bands based on the transfer function of a conceptual LTI system. The related theory of the LTI system and transfer function can be found in Text S1 in the Supporting Information S1.

To capture the total effects of ET and Pr on the SSM variability, we use a conceptual LTI system with the excitation as et(t) and $pr(t)$ together and the response as ssm(t) (Figure 2). Since ET and Pr have different spectral characteristics in the frequency domain (Katul et al., 2007; Nakai et al., 2014; also from Figure 3 in Section 3.1), here we separate their effects on SSM as two inputs and determine the total effects as an identical transfer function. Regarding this system as a "black-box" model, we can focus on the relationship between excitation (i.e., ET and Pr) and response (i.e., SSM) without consideration of the internal variations of the system. In this way, the relationship between ssm(t), et(t), and $pr(t)$ can be expressed as:

$$\text{ssm}(t) = et(t) * h_{\text{sep}}(t) + pr(t) * h_{\text{sep}}(t) \tag{3}$$
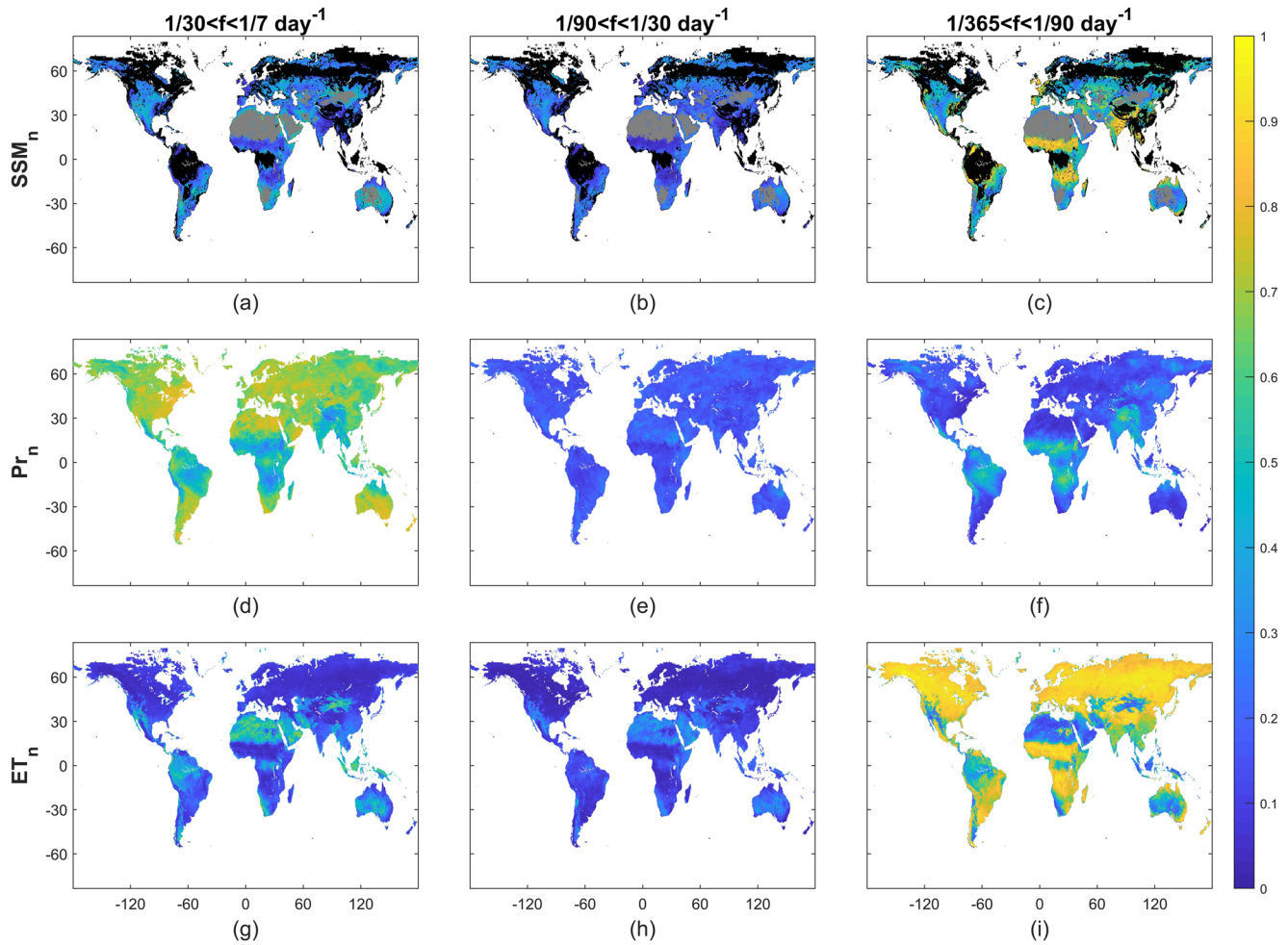
Figure 3. Surface soil moisture (SSM_n; Figures a–c), precipitation (Pr_n; Figures d–f), and evapotranspiration (ET_n; Figures g–i) based on the reference data over the three frequency bands. SSM_n, Pr_n, and ET_n are the normalized variability of SSM, Pr, and ET, respectively, defined in Section 2.5. Black parts in Figures (a–c) are regions where Soil Moisture Active Passive retrievals have potential errors defined in Section 2.2. Dark gray parts in Figures (a–c) are regions with SSM_n (defined in Section 2.7) less than 0.1. For all subsequent results, including Figure 3, the three columns from left to right represent the weekly to monthly frequency band ($n = 1$), the monthly to seasonal frequency band ($n = 2$), and the seasonal to annual frequency band ($n = 3$).

where $h_{sep}(t)$ is the transfer function of the LTI system shown in Figure 2. Then, Equation 3 can be expressed as the spectrum analysis in the frequency domain:

$$F_{SSM}(k) = F_{ET}(k) \cdot H_{SEP}(k) + F_{Pr}(k) \cdot H_{SEP}(k) \tag{4}$$

where $H_{SEP}(k)$ is the Fourier transform of the transfer function $h_{sep}(t)$. Thus, the variations of the excitation and response spectra of the LTI system are determined by the transfer function $H_{SEP}(k)$ as:

$$H_{SEP}(k) = \frac{F_{SSM}(k)}{F_{ET}(k) + F_{Pr}(k)} \tag{5}$$

where $F_{ET}(k)$, $F_{Pr}(k)$, and $F_{SSM}(k)$ are the Fourier transform (amplitude spectrum) of $et(t)$, $pr(t)$, and $ssm(t)$.

In order to separately characterize the total effects of ET and Pr on SSM variability within the three frequency bands, we calculate the normalized variability of SSM, Pr, and ET (SSM_n, Pr_n, and ET_n, as X_n in Figure 1). We aim to use X_n to indicate the proportion of the temporal variability over different frequency bands. The procedures to get SSM_n, Pr_n, and ET_n from time series of SSM ($ssm(t)$), Pr ($pr(t)$), and ET ($et(t)$) are shown in Figure 1 (see Figure S1 in the Supporting Information S1 for a detailed version). This method to process SSM_n has been applied in a previous study (Xi et al., 2022). The processing of Pr_n and ET_n follows a similar

procedure. We separate the filtered $E_X(k)$ ($E_X(k)'$ in Figure 1, see Section 2.4) into three frequency bands: weekly to monthly time scales ($7 \sim 30$ days), monthly to seasonal time scales ($30 \sim 90$ days), and seasonal to annual time scales ($90 \sim 365$ days). Finally, we define the normalized variability of X as the spectral power of each frequency band divided by the total spectral power of $E_X(k)'$:

$$X_{n_i} = \frac{\sum_j E_{X_i}(k_j)'}{\sum_{i=1}^{3} \sum_j E_{X_i}(k_j)'} \tag{6}$$

where $E_{X_i}(k_j)'$ represents the spectral power of X for the jth frequency in the ith frequency band, i is the ordinal number representing the three frequency bands from high to low, and j is the ordinal number of each frequency within each frequency band. Thus, we denote X_{n_i} as the normalized variability of X in the ith frequency band. In this way, X_{n_i}, as a value between 0 and 1, indicates the proportion of the temporal variability of $x(t)$ expressed in the ith frequency band.

Next, we reformulate Equation 5 based on the normalized variability:

$$H_{\text{SEP}_{n_i}} = \frac{\text{SSM}_{n_i}}{\text{ET}_{n_i} + Pr_{n_i}} \tag{7}$$

where $H_{\text{SEP}_{n_i}}$ is the fraction of SSM variability to the sum of ET and Pr variability (i.e., demand and supply) in the ith frequency band. The higher this ratio, the stronger effects on the temporal variability of SSM by ET and Pr. We also aim to define the dominant factor on SSM variability (i.e., either ET or Pr) within the three frequency bands. Therefore, we define another ratio:

$$H_{\text{EEP}_{n_i}} = \frac{\text{ET}_{n_i}}{\text{ET}_{n_i} + Pr_{n_i}} \tag{8}$$

where $H_{\text{EEP}_{n_i}}$ is the fraction of ET variability to the sum of ET and Pr variability in the ith frequency band. This ratio is greater than one-half means that ET has larger variability than Pr and thus a greater impact on the temporal variability of SSM and vice versa. In this way, we use $H_{\text{SEP}_{n_i}}$ and $H_{\text{EEP}_{n_i}}$ as two indicators to characterize the effects of ET and Pr on SSM variability in the three frequency bands. $H_{\text{SEP}_{n_i}}$ measures the total effect of ET and Pr on SSM variability and $H_{\text{EEP}_{n_i}}$ determines which water flux (i.e., Pr or ET) is dominant. A detailed procedure to get $H_{\text{SEP}_{n_i}}$ and $H_{\text{EEP}_{n_i}}$ can be found in Figure S1 in the Supporting Information S1.

2.6. Analysis of Spectral Slope of SSM, Pr, and ET

The spectral slopes of time series can explain how ET and Pr variability contribute to the spectrum of soil moisture (Katul et al., 2007). A common way to characterize the spectral slope is the power-law noise, which is the noise distributed in the whole frequency domain and with the form that variance scales with frequency according to an inverse power law (Mandelbrot, 1982). Being considered power-law noise, the spectral densities of time series vary as proportional to $1/f^\beta$ (i.e., inverse frequency), where β is the inverse number of the spectral slope (Bourke, 1998). In this way, the spectra of SSM, Pr, and ET time series can be used to characterize different noises and categorize noises into different "colors" based on the spectral slopes. The basic theory of the color of noise can be found in Text S2 in the Supporting Information S1.

The spectral slopes for SSM ($\text{SSM}_{k\omega i}$), Pr ($Pr_{k\omega i}$), and ET ($ET_{k\omega i}$) are approximated from the $E_X(k)'$ (gotten from Section 2.4) based on the linear regression, as the orange dashed box shown in Figure 1. In this study, we use white noise and five main colored noises (violet, blue, pink, red, and black noise) to characterize $X_{k\omega i}$ in the ith frequency band. The corresponding spectral slope (i.e., the opposite of β in inverse power law $1/f^\beta$) of violet, blue, white, pink, and red noise (or Brownian noise) is 2, 1, 0 (i.e., the spectral density of white noise is flat), -1, and -2, respectively, and the spectral slope of black noise is smaller than -2 (see Table S4 in the Supporting Information S1). The smaller the spectral slope in the frequency domain, the longer the memory of the signals represented as different colors of noise (excluding violet and blue noise). For example, a signal with its spectrum shown as white noise means the contribution to its variance is equal across all frequencies, while a signal with its spectrum shown as red noise means low-frequency periodic components dominate the contribution to its variance.

2.7. Analysis of Differences Between CMIP5 Models and Reference Data

We evaluate the multimodel differences of $H_{\mathrm{SEP}n}$ and $H_{\mathrm{EEP}n}$ within CMIP5 compared to reference data (i.e., SMAP and ERA5) by subtracting reference data from CMIP5 averages. In addition, we calculate the coefficient of variation across 14 models to examine inter-model variability.

The spatial resolution and the land cover between CMIP5 models and reference data, as well as among models themselves, are different. Here we re-grid all results with the same spatial resolution and land cover as SMAP so that they can be compared with each other. Specifically, we first project all matrices to the same spatial resolution as SMAP (36 km × 36 km) based on the nearest neighbor search, that is, find the closet pixel within each spatial resolution compared to SMAP resolution and let the value of that closet pixel as the value for the corresponding pixel in SMAP resolution. Then, for each re-gridded matrix, we fill those pixels without valid values (i.e., shown as "NaN") but have values in SMAP data with the mean values of their nearest neighbors. We also removed the pixels (i.e., set to "NaN") without a valid value in the corresponding SMAP resolution. In this way, all re-gridded matrices have the same land cover as the results based on SMAP data.

In addition, we test the robustness of the multimodel differences within CMIP5 compared to SMAP and ERA5 references to avoid the cases where differences are caused by only a few models or even one model. This robustness of the differences is depicted on the maps using stippling, showing the regions with a fraction of models as 100% (i.e., all 14 models agree on the sign of average differences) and 75% (i.e., 11 of the 14 models agree on the sign of average differences). Finally, since the variation of soil moisture in dry regions is usually very small (Koster et al., 2009), we remove regions with $\overline{\mathrm{SSM}}_n$ less than 0.1, where $\overline{\mathrm{SSM}}_n$ is the spatiotemporal normalized mean SSM based on SMAP (Figure S3 in the Supporting Information S1). To get $\overline{\mathrm{SSM}}_n$, we first use SMAP SSM retrievals to get the daily mean SSM ($\overline{SSM}$) for each pixel. Then we normalize them between zero and one based on the min-max normalization as:

$$\overline{\mathrm{SSM}}_n = \left(\overline{\mathrm{SSM}} - \overline{\mathrm{SSM}}_{\min} \right) / \left(\overline{\mathrm{SSM}}_{\max} - \overline{\mathrm{SSM}}_{\min} \right) \tag{9}$$

where $\overline{\mathrm{SSM}}_{\min}$ and $\overline{\mathrm{SSM}}_{\max}$ are the minimum and maximum $\overline{\mathrm{SSM}}$ on the global scale.

3. Results and Discussion

3.1. Temporal Variabilities of Soil Moisture, Precipitation, and Evapotranspiration From SMAP and ERA5 Reference Data

The temporal variability of SSM (SSM_n) is larger in the seasonal to annual frequency band in most regions, with a smaller proportion in the two higher frequency bands, indicating that SSM has large variability on time scales longer than the seasonal time scale (Figures 3a–3c).

The temporal variability of precipitation (Pr_n) shows different regional distributions over the three frequency bands (Figures 3d–3f). The variability is larger in the lowest frequency band for most tropical regions where the seasonal cycle can be large, and is larger in the highest frequency band for other regions, especially non-tropical regions. The reason is that, in most tropical regions, especially regions with tropical wet and dry climate, like Brazil, India, Northern Australia, and regions between the Sahara Desert and the equator in Africa, although the variation of temperature and radiation are small over a year, rainfall exhibits a strong seasonal cycle—the days with and without rainfall are concentrated so that the boundaries of the wet season and dry season are more distinct. So, precipitation in these regions shows a large seasonal variability. However, in tropical regions with a very wet climate, such as the Democratic Republic of the Congo and Indonesia, there is no such seasonality because of the more steady rainfall pattern in these regions. Regions right along the equator usually have two rainy seasons corresponding to both equinoxes. On the other hand, there is no obvious wet and dry season distinction for most non-tropical regions. The occurrence of rainfall is typically more random over a whole year and close to a white noise signal at high frequencies (Katul et al., 2007; Nakai et al., 2014). Therefore, precipitation variability in non-tropical regions is almost all high-frequency variability, except for regions with a Mediterranean climate and monsoonal regions where the monsoon distributes rainfall in a few months, imposing a strong seasonal cycle.

The temporal variability of ET (ET_n) is largest in the seasonal to annual frequency band over most regions except for regions with a tropical wet climate (Figures 3g–3i). The reason is that ET in most regions is driven by either
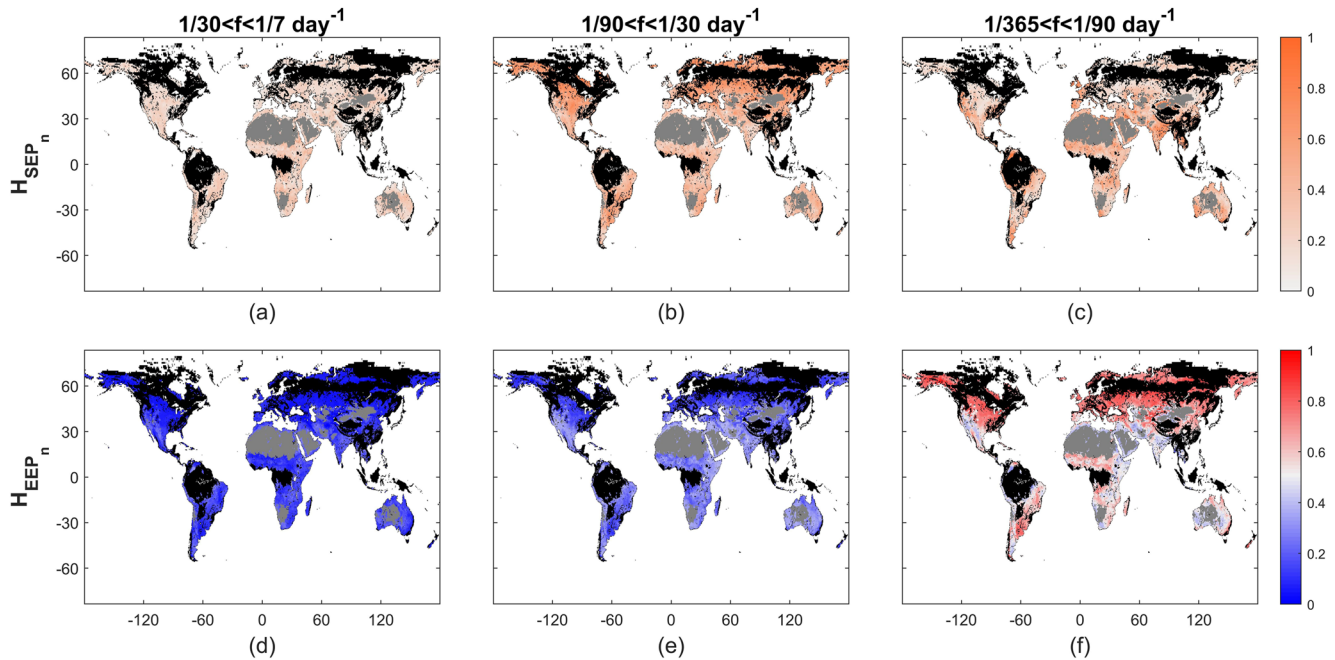
Figure 4. H_{SEP_n} (Figures a–c) and H_{EEP_n} (Figures d–f) based on the reference data over the three frequency bands. H_{SEP_n} is the ratio of Surface soil moisture (SSM_n) to the sum of evapotranspiration (ET_n) and precipitation (Pr_n), and H_{EEP_n} is the ratio of ET_n to the sum of ET_n and Pr_n, defined in Section 2.6. The values within each frequency band are normalized to between zero and one across the three frequency bands. Black parts are regions where Soil Moisture Active Passive retrievals have potential errors. Dark gray parts are regions with $\overline{SSM_n}$ less than 0.1.

radiation or moisture limitation with high seasonality, except in the wet tropics where the seasonality of radiation and moisture is small but the daily variability can be large. In this way, the results in tropical wet regions, such as in the Amazon rainforest, Africa's Equator, Indonesia, and the Philippines, are the opposite of other regions in terms of frequency distribution, showing ET variability is concentrated on time scales shorter than monthly. This high-frequency radiation variability is mainly due to the variability of clouds on daily to weekly time scales which causes a large variability of ET on these short time scales (Anber et al., 2015). Moreover, this mechanism has the largest influence on regions near the equator because these regions receive more radiation than other regions over a year and thus have larger variations between incoming solar radiation on cloudy versus non-cloudy days. Therefore, in these regions, large ET variability is mostly located in the highest frequency band. In addition, ET in very dry regions (e.g., deserts) does not have a clear seasonal cycle as well due to the strong limitation of moisture.

Figure 4 shows the global distribution of H_{SEP_n} and H_{EEP_n} based on SMAP and ERA5 data over the three frequency bands (the corresponding values of H_{SEP_n} and H_{EEP_n} in each frequency band see Table S5 in the Supporting Information S1). In the weekly to monthly frequency band, the total effect of ET and Pr on SSM variability is less than in the other two frequency bands. Compared to Pr, which is the dominant driver of SSM variability in this frequency band, the fluctuation of ET has limited effects on SSM as ET has less variability, in part regulated by soil moisture itself (Figures 4a and 4d). On time scales longer than monthly, ET and Pr together have more effects on SSM variability. In the monthly to seasonal frequency band where the total effect of ET and Pr on SSM reaches its largest magnitude, although the proportion of ET variability becomes larger, Pr is still the dominant factor of SSM variability (Figures 4b and 4e). In the seasonal to annual frequency band, the total variability of ET and Pr decreases but is still larger than that in the weekly to monthly frequency band. However, in this frequency band, ET becomes the dominant factor on SSM, especially in middle and high latitudes. Therefore, Pr variability alone in these regions is no longer able to explain the SSM dynamics, and the seasonality of ET has to be considered (Figures 4c and 4f). Since H_{EEP_n} represents the proportion of ET variability to the total variability of ET and Pr, similar to ET_n shown in Figure 3, H_{EEP_n} patterns are different in tropical wet regions, where ET variability has more effects on SSM on the two higher frequency bands (Figures 4d and 4e), and Pr becomes the dominant factor on the lowest frequency band due to the strong seasonality of rainfall (Figure 4f).

To further identify the Pr and ET effects on SSM variability, we evaluate the relationships between their spectral slopes. Figure 5 shows the global distribution of SSM_{kw}, Pr_{kw}, and ET_{kw} expressed in terms of noise color in the
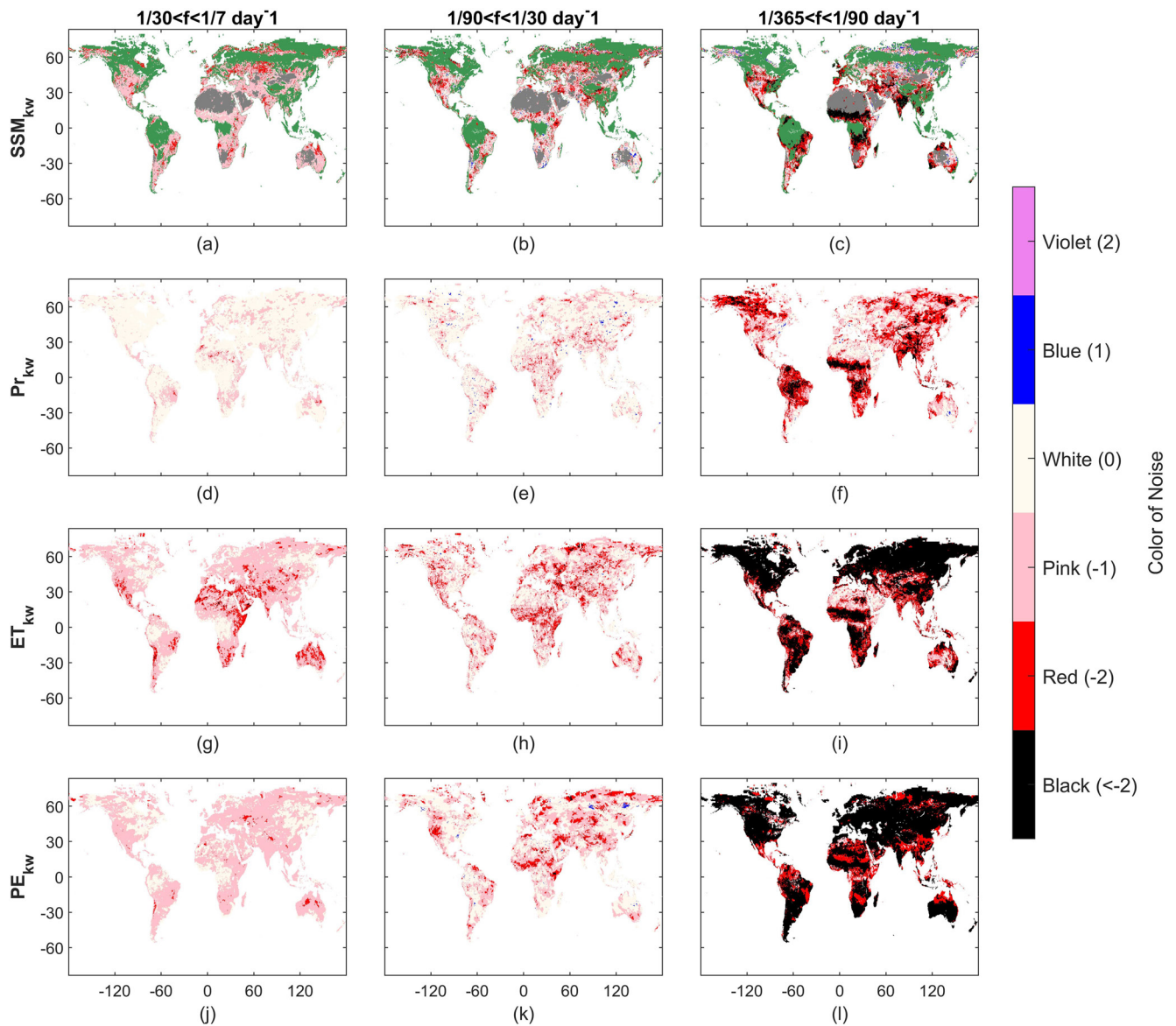
Figure 5. Noise color of surface soil moisture (SSM) (Figures a–c), precipitation (Pr) (Figures d–f), evapotranspiration (ET) (Figures g–i), and potential evaporation (PE) (Figures j–l) over the three frequency bands according to SSM_{kw}, Pr_{kw}, ET_{kw}, and PE_{kw} based on the reference data. The colors in each figure represent the corresponding color of noise, referring to the power spectra of SSM, Pr, ET, and PE. The colorbar shows the color referring to each noise, and the number in brackets is the spectral slope of power-law noise corresponding to each noise color. Green and dark gray parts in Figures (a–c) are regions where Soil Moisture Active Passive retrievals have potential errors and regions with $\overline{SSM_n}$ less than 0.1, respectively.

three frequency bands based on SMAP and ERA5 data. We also evaluate the spectral slope of potential evaporation (PE_{kw}) from ERA5 to compare it with ET_{kw}.

From a previous study (Xi et al., 2022), we have found that the low-frequency periodic components dominate the variance of SSM, and it has more randomness on time scales shorter than monthly and more memory on time scales longer than seasonality. From Figures 5a–5f, we further find that there is a phase shift between SSM and Pr spectra in the two higher frequency bands, especially the highest one, which implicates how Pr variability propagates into the soil moisture system (Katul et al., 2007). In the weekly to monthly frequency band where Pr is the dominant factor on SSM (according to Figure 4d), regions with smaller Pr_{kw} lead to SSM spectra that decay more rapidly. In most regions where Pr is similar to a white noise process, SSM exhibits a pink noise process in the corresponding regions, indicating longer memory induced by soil moisture (Salvucci & Entekhabi, 1994). In regions where Pr exhibits a pink noise process, like eastern Africa, eastern Brazil, western India, and northern

Australia, SSM has a red noise spectrum (Figures 5a and 5d). A similar relationship between SSM and Pr spectra can also be found in the monthly to seasonal frequency band (Figures 5b and 5e), such as in southern North America, eastern India, and southern Somali Peninsula, but it is not as evident as that in the highest frequency band since the effect of Pr on SSM variability decreases in this frequency band (according to Figure 4e). In the seasonal to annual frequency band, ET exerts more effects on SSM variability than Pr for most regions (according to Figure 4f), so there are no strong correlations between Pr and SSM spectra. In previous studies, soil moisture was found to be similar to a red or black noise corresponding to precipitation having a white or pink noise at high frequency (Katul et al., 2007; Nakai et al., 2014). The SSM_{kw} here is a little larger (Figure 5a). The main reason could be the random errors from remote sensing retrievals (i.e., SMAP here). Remotely sensed SM retrievals usually have stochastic errors that can be mainly extracted from high-frequency noise (Su et al., 2014). This random noise could increase the high-frequency components of the SSM signal and thus reduce "redness" within the first frequency band of the SSM spectra derived from SMAP retrievals (see Figure S6 in Supporting Information S1). Previous studies (e.g., Delworth & Manabe, 1988; Katul et al., 2007) based on water-balance models tend to have fewer random errors than signals from remote sensing retrievals, thus exhibiting a soil moisture signal similar to red noise.

Unlike between SSM_{kw} and Pr_{kw}, there is no such relationship between SSM_{kw} and ET_{kw}, even at the highest frequency band where ET is dominant on SSM variability (Figures 5a–5c and 5g–5i). We find that Pr and ET exert strong effects on SSM variability in different ways across different time scales. In previous studies, unlike Pr serving as a forcing term, ET was shown to be related to the damping term of soil moisture spectra (Delworth & Manabe, 1988; Katul et al., 2007; Nakai et al., 2014), which modulates potential evaporation (PE). The differences between ET_{kw} and PE_{kw} are mainly due to the variability of soil moisture. PE is an estimate of the maximum evaporation rate from a surface of pure water for given meteorological conditions (Delworth & Manabe, 1988). Weather fluctuations introduce a white or pink noise PE. However, unlike PE, ET is closely related to soil moisture, emphasizing that soil moisture limits and regulates the supply of moisture to the atmosphere on longer time scales. So the SSM dynamics influence ET spectra—leading to a redder noise than PE spectra because SSM has a longer memory. This influence is especially more visible in dry regions. The reason is that, compared to SSM in dry regions, SSM in wet regions mostly tracks the variability of PE. So ET in wet regions will not be strongly affected by SSM variability and thus still shows pink noise. On longer time scales, both ET and PE show obvious seasonality, with low-frequency periodic components dominating the contribution to the variance of signals (Figures 5i and 5l).

To summarize, the effects of Pr and ET on SSM variability are different across time scales. In the two higher frequency bands (especially the weekly to monthly frequency band), Pr, acting as a forcing by averaging the large oscillations to limit high-frequency components, has more effect on SSM variability. In the seasonal to annual frequency band, ET, acting as a dissipative process that prevents SSM anomalies from persisting indefinitely, has more effects on SSM variability.

3.2. Comparison Between CMIP5 Simulations and SMAP and ERA5 References

Figures 6a–6c shows the average differences for H_{SEPn} and H_{EEPn} of model simulations within CMIP5 compared to SMAP and ERA5 data. The robustness of the multimodel differences is characterized by the consistency of the sign within CMIP5. As described in Section 2.7, the "+" stippling means all 14 models (100%) agree on the sign of average differences and the "." stippling means 11 of the 14 models (75%) agree on the sign of average differences. Therefore, we only focus on the regions with stippling. For most regions, the multimodel differences of H_{SEPn} are negative in the two higher frequency bands and they are positive in the lowest frequency band, which means that the CMIP5 simulations of the total effect of ET and Pr on SSM variability are smaller on time scales shorter than seasonal and are larger on time scales longer than seasonal, compared to SMAP and ERA5 data (Figures 6a–6c). The average difference of H_{SEPn} is largest in the monthly to seasonal frequency band (−0.5898 and −0.3797 with 100% and 75% fraction of models) and smallest in the weekly to monthly frequency band (−0.2816 and −0.2366 with 100% and 75% fraction of models) (Table 1). For all three frequency bands, the average differences of H_{SEPn} are larger in Northern North America and Central Asia.

From Section 3.1, we know that Pr dominates SSM variability in the two higher frequency bands, and ET dominates it in the seasonal to annual frequency band. From Figures 6e–6f, we find that in each frequency band, the effect of the corresponding dominant factor (i.e., Pr or ET) on SSM simulated within the CMIP5 models tends to be smaller than that from ERA5 reference. Specifically, in the two higher frequency bands where Pr is the dominant factor,
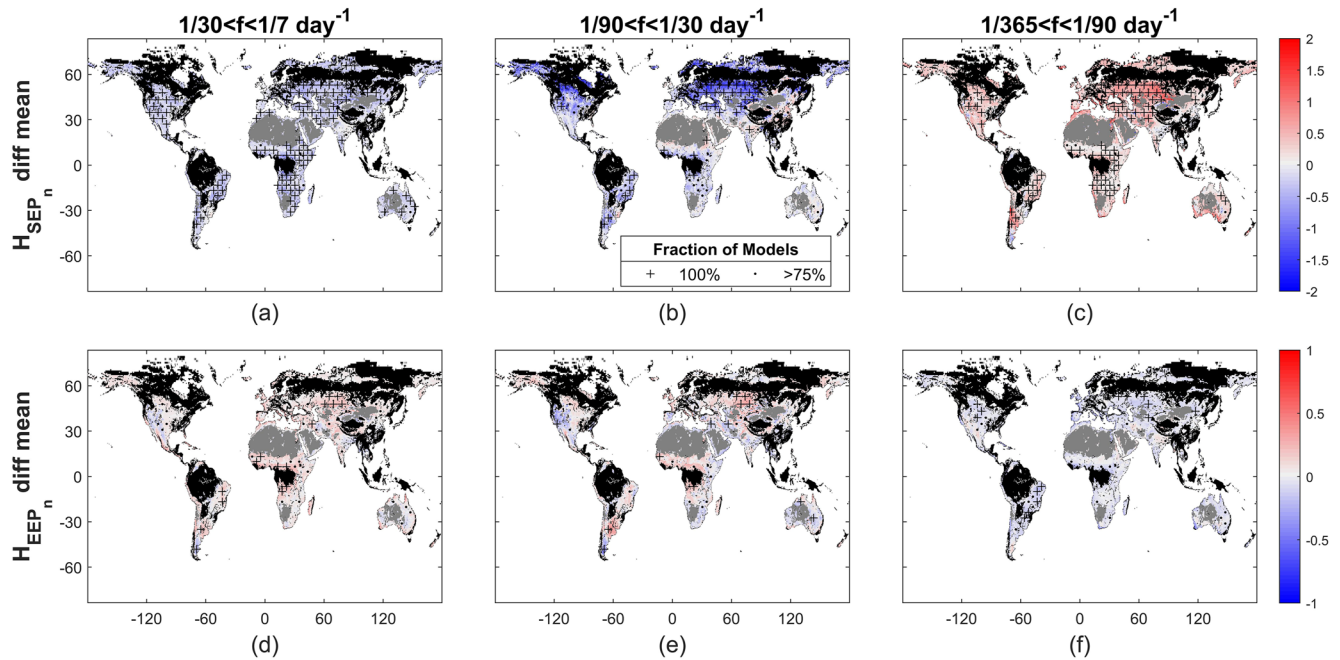
Figure 6. Average differences of H_{SEP_n} (Figures a–c) and H_{EEP_n} (Figures d–f) between Coupled Model Intercomparison Project Phase 5 (CMIP5) models and the reference data (Soil Moisture Active Passive (SMAP) and ECMWF Reanalysis v5 (ERA5)) in the three frequency bands. The differences are calculated by subtracting reference data from CMIP5 averages. Black parts are regions where Soil Moisture Active Passive retrievals have potential errors. Dark gray parts are regions with $\overline{SSM_n}$ less than 0.1. For each figure, "+" and "." stippling represents the region with a fraction of models as 100% and 75% for a robustness test described in Section 2.7.

Table 1
Multimodel Differences of H_{SEP_n} Within CMIP5 and H_{SEP_n} From Reference Data

Fraction of models	100% (14/14)			75% (11/14)		
Frequency band (day^{-1})	1/7 ~ 1/30	1/30 ~ 1/90	1/90 ~ 1/365	1/7 ~ 1/30	1/30 ~ 1/90	1/90 ~ 1/365
BCC-CSM1.1	−0.2287	−0.4913	0.5263	−0.1797	−0.2514	0.4390
BNU-ESM	−0.2644	−0.5324	0.4257	−0.2213	−0.3412	0.3562
CanESM2	−0.2971	−0.6219	0.4756	−0.2497	−0.3763	0.3763
CNRM-CM5	−0.2682	−0.7112	0.4033	−0.2177	−0.5247	0.3198
CSIRO-Mk3.6	−0.3105	−0.6783	0.4514	−0.2672	−0.4772	0.3891
GFDL-CM3	−0.2667	−0.5615	0.3372	−0.2253	−0.3613	0.2606
GFDL-ESM2G	−0.2677	−0.5642	0.4042	−0.2256	−0.3703	0.3192
GFDL-ESM2M	−0.2667	−0.5565	0.4074	−0.2244	−0.3621	0.3203
MIROC5	−0.2846	−0.4983	0.3245	−0.2406	−0.2782	0.2526
MIROC-ESM	−0.2902	−0.5568	0.3558	−0.2461	−0.3409	0.2847
MIROC-ESM-CHEM	−0.2905	−0.5592	0.3531	−0.2464	−0.3429	0.2825
MRI-CGCM3	−0.3216	−0.6953	0.4958	−0.2763	−0.4888	0.4324
MRI-ESM1	−0.3197	−0.6935	0.4944	−0.2747	−0.4842	0.4304
NorESM1-M	−0.2659	−0.5364	0.3800	−0.2178	−0.3163	0.2995
Average (±1 SD)	−0.2816 ± 0.0246	−0.5898 ± 0.0728	0.4168 ± 0.0618	−0.2366 ± 0.0252	−0.3797 ± 0.0798	0.3402 ± 0.0619
Reference	0.4273	1.0051	0.4731	0.3898	0.8563	0.5288

Note. The reference H_{SEP_n} here is the original value without normalization across the three frequency bands.

Table 2
Multimodel Differences of H_{EEP_n} Within CMIP5 and H_{EEP_n} From Reference Data

| Fraction of models	100% (14/14)			75% (11/14)		
Frequency band (day^{-1})	$1/7 \sim 1/30$	$1/30 \sim 1/90$	$1/90 \sim 1/365$	$1/7 \sim 1/30$	$1/30 \sim 1/90$	$1/90 \sim 1/365$
BCC-CSM1.1	0.2056	0.0994	−0.1234	0.1599	0.0995	−0.0732
BNU-ESM	0.2101	0.0765	−0.1571	0.1534	0.0657	−0.1278
CanESM2	0.1305	0.1270	−0.0900	0.0843	0.1261	−0.0638
CNRM-CM5	0.1028	−0.0034	−0.0728	0.0532	−0.0127	−0.0396
CSIRO-Mk3.6	0.1017	0.0443	−0.0833	0.0509	0.0364	−0.0569
GFDL-CM3	0.1304	0.0370	−0.0915	0.0758	0.0315	−0.0657
GFDL-ESM2G	0.1846	0.0836	−0.1112	0.1273	0.0789	−0.0841
GFDL-ESM2M	0.1821	0.0807	−0.1068	0.1224	0.0758	−0.0786
MIROC5	0.0938	−0.0196	−0.0559	0.0198	−0.0437	−0.0225
MIROC-ESM	0.1396	0.0333	−0.0777	0.0719	0.0219	−0.0541
MIROC-ESM-CHEM	0.1386	0.0323	−0.0784	0.0704	0.0218	−0.0542
MRI-CGCM3	0.1411	0.0621	−0.0664	0.0851	0.0524	−0.0382
MRI-ESM1	0.1396	0.0636	−0.0658	0.0838	0.0542	−0.0370
NorESM1-M	0.1594	0.0285	−0.1062	0.0997	0.0207	−0.0840
Average (±1 SD)	0.1471 ± 0.0357	0.0532 ± 0.0381	−0.0919 ± 0.0260	0.0899 ± 0.0380	0.0449 ± 0.0425	−0.0628 ± 0.0255
Reference	0.1757	0.4330	0.8130	0.2127	0.4083	0.7709

Note. The reference H_{EEP_n} here is the original value without normalization across the three frequency bands.

CMIP5 models have a larger ET influence. Thus, the effects of Pr on SSM within CMIP5 are smaller compared to the references (Figures 6d–6e). In the lowest frequency band where ET is the dominant factor, CMIP5 models estimate smaller effects of ET on SSM compared to the references. Unlike H_{SEP_n}, the multimodel difference of H_{EEP_n} is largest in the weekly to monthly frequency band (0.1471 and 0.0899 with 100% and 75% fractions of models) and smallest in the monthly to seasonal frequency band (0.0532 and 0.0449 with 100% and 75% fraction of models) (Table 2). In addition to examining multimodel differences, we also investigate the coefficient of variation (CV) of H_{SEP_n} and H_{EEP_n} across CMIP5 models to see their statistical variances (Figure S4 in the Supporting Information S1). For both H_{SEP_n} and H_{EEP_n}, the intermodel spread is larger in the weekly to monthly and monthly to seasonal frequency band and smaller in the seasonal to annual frequency band (also see Table S6 in the Supporting Information S1). Therefore, for the simulated Pr and ET effects on SSM variability within CMIP5, there is a more extensive intermodel spread on time scales shorter than seasonal and a lower variance among models on time scales longer than seasonal time scale, suggesting an individual difference in representing the short-term variability and a systematic difference of these CMIP5 models in representing the long-term variability compared to the reference data.

The multimodel differences of H_{SEP_n} and H_{EEP_n} are further analyzed with $\overline{SSM}_n$ (defined in Section 2.7) on a global scale. To make a trade-off between strong robustness and the size of samplings, we use the differences where 75% of models agree on the sign of multimodel differences. For H_{SEP_n} (Figures 7a–7c), the multimodel differences are similar in the weekly to monthly frequency range and seasonal to annual frequency range—the smallest differences appear in the regions with $\overline{SSM}_n$ from 0.6 to 0.85. In the monthly to seasonal frequency band, apart from the regions same as those in the other two frequency bands, the extremely dry regions ($\overline{SSM}_n$ from 0 to 0.05) also show the smallest differences. In all three frequency bands, the largest differences appear in the extremely wet regions ($\overline{SSM}_n$ from 0.95 to 1). For H_{EEP_n} (Figures 7d–7f), the relationships between its multimodel differences and $\overline{SSM}_n$ are similar across all of the three frequency bands—the differences are larger in the regions with $\overline{SSM}_n$ from 0.1 to 0.7 and are smaller in both extremely dry and wet regions.

3.3. Uncertainty Analysis and Discussion

Since the SMAP SSM retrievals are non-continuous on the daily time scale, we fill in the missing values before performing Fourier analysis. The gap-filling process is the same as our previous study and has been carefully
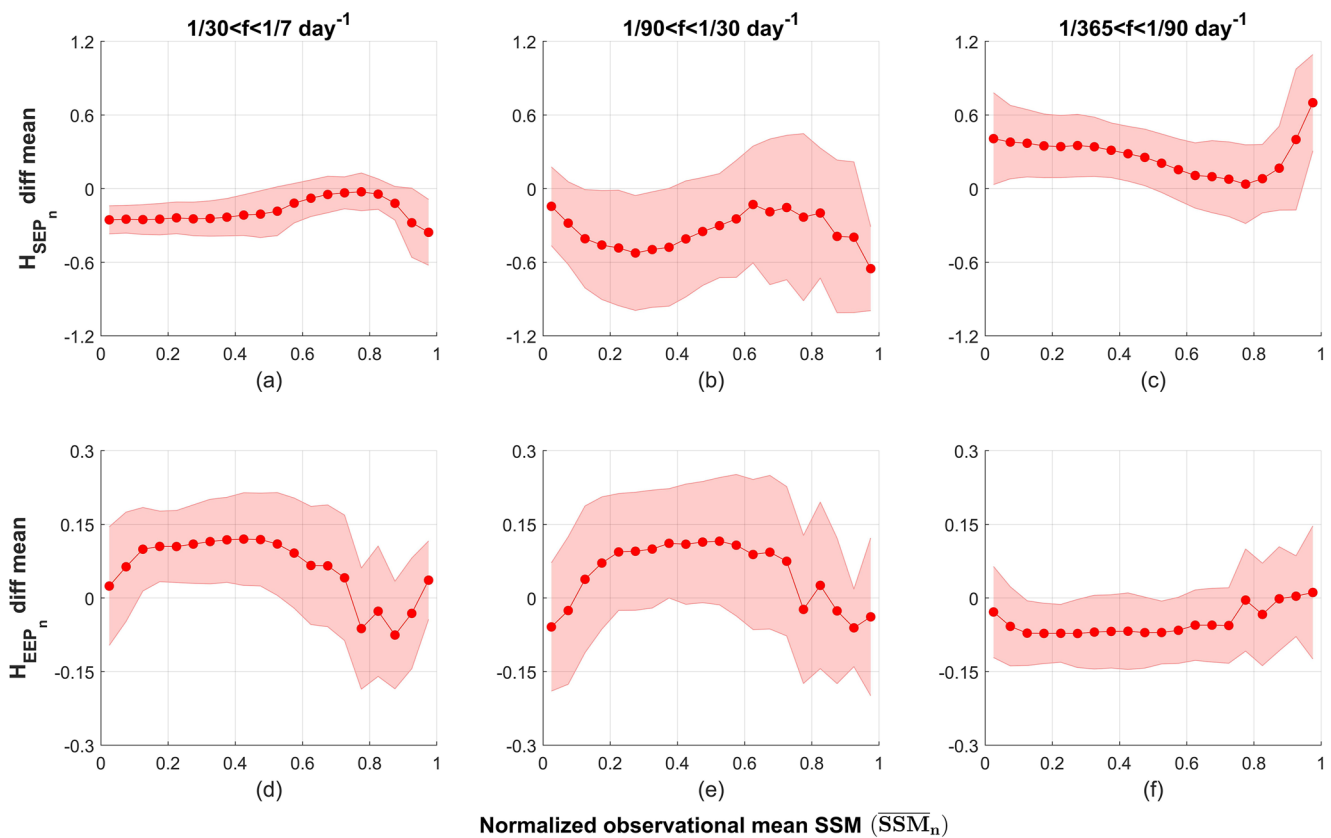
Figure 7. Comparison of average differences of H_{SEP_n} (Figures a–c) and H_{EEP_n} (Figures d–f) between Coupled Model Intercomparison Project Phase 5 (CMIP5) models and reference data (Soil Moisture Active Passive (SMAP) and ECMWF Reanalysis v5 (ERA5)) with $\overline{SSM}_n$ in the three frequency bands. The red shading represents +/− one standard deviation. $\overline{SSM}_n$ is first separated into 20 bins of equal size (i.e., 0.05 for each bin), then the mean and standard deviation of H_{SEP_n} and H_{EEP_n} differences located in each bin (corresponding to the range of $\overline{SSM}_n$) were separately calculated for each frequency band. Differences in this figure are the values with a 75% model of fraction for a robustness test. All values in the regions where SMAP retrievals have potential errors and $\overline{SSM}_n$ less than 0.1 are removed.

validated using in situ soil moisture data from ISMN (Xi et al., 2022). Although the gap-filled results perform well compared to in situ data according to statistical error analysis, we do not have observations for missing values of all pixels globally. Therefore, we would like to quantify the uncertainties due to this gap-filling process. Among the four parameters during this process (moving average or moving median, moving window length, maximum length of prediction sequences, and autoregressive model order), we find that $\overline{SSM}_n$ is more sensitive to the "moving window length" (see Figure S5 in the Supporting Information S1). Thus, the constraint of uncertainties from this parameter is the most critical.

To test the effects by the "moving window length", we set it as 3, 5, 7, and 9 days, respectively, and fix the other three parameters to calculate SSM_n from SMAP. We find that the change of SSM_n due to this parameter is more evident in the first and the third frequency band (see Table 3). As the "moving window length" increases, SSM_n in the first frequency band will decrease since the moving window here performs like a low-pass filter that will decrease the components of higher frequencies. Correspondingly, SSM_n in the third frequency bands will increase. However, even though setting the "moving window length" as 9, the multimodel mean of SSM_n within CMIP5 is still smaller than SSM_n from SMAP in the first two frequency bands and larger than that in the third frequency band. This indicates that the choice of the parameter during the gap-filling process will not affect the relative size between SSM_n from SMAP and CMIP5. In addition, during the gap-filling process of SMAP retrievals, we first use a long term global daily soil moisture data set named NNsm (see Section 2.3) to fill in the missing values. Since SSM data filled with NNsm are still discontinuous at the daily time scale, we set the "moving window length" as 3, 5, 7, and 9 again for that NNsm-filled data set. We find that filled by NNsm, the uncertainties of SSM_n from SMAP due to the choice of the gap-filled parameter are constrained across the three frequency bands, especially in the first frequency band where the relative change is the largest among different

Table 3
Normalized Variability of SSM (SSM$_n$) From Two Observation-Based Data Sets With Different Moving Window Lengths and CMIP5 Model Average in Three Frequency Bands

Data sets	Moving window length (#)	Normalized variability of SSM (SSM$_n$) in three frequency bands		
		$1/7 \sim 1/30$ days^{-1} (weekly to monthly)	$1/30 \sim 1/90$ days^{-1} (monthly to seasonal)	$1/90 \sim 1/365$ days^{-1} (seasonal to annual)
SMAP	3	0.2698	0.2125	0.5177
	5	0.2523	0.2162	0.5315
	7	0.2367	0.2190	0.5444
	9	0.2102	0.2228	0.5670
(Relative change)		22.09%	4.85%	9.52%
SMAP and NNsm	3	0.2833	0.2050	0.5117
	5	0.2710	0.2090	0.5201
	7	0.2564	0.2126	0.5310
	9	0.2418	0.2151	0.5431
(Relative change)		14.65%	4.92%	6.13%
CMIP5 model average		0.1224	0.1445	0.7330

Note. The regions where SMAP retrievals have potential errors and $\overline{SSM}_n$ less than 0.1 are removed. The "relative change" is the relative change from the shortest to the longest moving window length for the two observation-based data sets.

choices (see Table 3). Moreover, from Table 3, we also find that filled by NNsm, SSM$_n$ increase in the first frequency band and decrease in the third frequency band. This means that SSM$_n$ from SMAP tends to be larger in the first frequency band and smaller in the third frequency band by adding more observation-based data, which is the same trend as decreasing the "moving window length." Therefore, we set the "moving window length" as 3 during the gap-filling process.

Apart from this technical issue, the linear and time-invariant assumption of the interactions among SSM, Pr, and ET could be another source of uncertainties. In this study, we assumed an LTI system for SSM, Pr, and ET and then performed the Fourier analysis. However, the relationships among them may not be linear and time-invariant. For example, in regions with plenty of vegetation, precipitation is first intercepted by the canopy, and then throughfall is further partitioned into surface runoff and infiltration water, which directly affects SSM instead of precipitation. A previous study has also shown that there is a higher linear relationship between soil moisture and precipitation in less-vegetated regions (Sehler et al., 2019). Snow is another factor related to this issue. When the precipitation is snow, it will not interact with SSM immediately. Instead, there is a snow accumulation and melting process, which could take days, weeks, and even months. Thus, the relationship between SSM and Pr may not be time-invariant in high-latitude regions. In addition, in regions where soil moisture is quite limited, the ET is also quite limited and thus has almost no effects on soil moisture. Basically, uncertainties from the LTI assumption could be mainly from regions with high vegetation, low temperature, and low soil moisture. As we described in Sections 2.2 and 2.7, we performed masks to remove values in dense vegetation cover regions, frozen landscapes, and areas with little soil moisture. Therefore, we removed those regions where the LTI assumption could induce high uncertainties when analyzing the relationships between SSM, Pr, and ET (i.e., H_{SEPn} and H_{EEPn}). In this way, although the LTI assumption made in this study is still not completely true, the uncertainties in our results from this aspect have been largely constrained.

Finally, remotely sensed soil moisture (e.g., SMAP SSM retrievals) is known to exhibit spurious spectral characteristics due to random retrieval errors (Su et al., 2014). These spurious features would have a significant impact on the high-frequency portion of the SMAP SSM spectra. We have discussed the consequence of reduced "redness" in the first frequency band derived from SMAP SSM signals made by this issue in Section 3.1. Here we also would like to discuss how the effects of Pr and ET on SSM will be influenced by this issue. Since the computation of H_{EEPn} does not involve SSM, we only consider the impacts on H_{SEPn}. Since the basic scientific requirement of SMAP is to provide SSM estimates with an error of no greater than 0.04 cm^3/cm^3 globally (Chan, 2016), we perform a test to compare H_{SEPn} between using original SMAP retrievals and new SMAP retrievals by adding

this random error. Specifically, for SMAP SSM in each pixel, we add a value randomly obtained from a normal distribution whose mean is the original SMAP retrieval and the standard deviation is 0.04 as the random error for that SSM retrieval. Then we perform the same process to get H_{SEP_n} using the new SMAP retrievals with random errors. We found that, by adding random errors, H_{SEP_n} increases in the first frequency band and decreases in the second and third frequency bands (see Figure S7 and Table S7 in the Supporting Information S1). However, adding random errors does not change the size relationship between CMIP5 models and reference data: CMIP5 simulations of the total effect of ET and Pr on SSM variability are smaller on the weekly to seasonal frequency band and are larger on the seasonal to annual frequency band, compared to SMAP and ERA5 data.

4. Conclusions

This study uses satellite-based reference data (SMAP and ERA5) to evaluate 14 ESMs within CMIP5 in simulating the effects of Pr and ET on SSM variability across three frequency bands. We find that compared to the reference data, the total effects of Pr and ET on SSM simulated within CMIP5 are smaller in the high-frequency bands (weekly to monthly and monthly to seasonal) and larger in the low-frequency band (seasonal to annual). Additionally, based on the findings that Pr dominates weekly to seasonal SSM variability and ET dominates seasonal to annual SSM variability, these CMIP5 models tend to estimate smaller effects on SSM by Pr or ET as the dominant factor in each frequency band compared to the reference data. Across the three frequency bands, the differences between CMIP5 models and the reference data are smaller in regions with strong land-atmosphere interactions between the three variables. For the metrics investigated here, there are individual multimodel differences in representing short-term variability and systematic multimodel differences in long-term variability.

This study also identifies systematic metrics that can be used to assess model performance and help refine process representation across time scales. Our results highlight that the precipitation and evapotranspiration effects on soil moisture differ from lower to higher frequency bands, and the CMIP5 models have differences with satellite-based reference in representing these effects. One limitation is that the analysis of this study can not explicitly show the accuracy of modeled Pr and ET compared to observations. Thus, we cannot tell whether Pr or ET is more accurately simulated within the ESMs. The uncertainties can be from both Pr and ET simulations, impacting their simulated effects on SSM. Quantifying the contribution of uncertainties from each contributor in future work shall improve the model performance in simulating soil moisture.

Data Availability Statement

The codes and data for analysis in this study are available via doi: https://doi.org/10.4231/whj3-kn14 in Purdue University Research Repository.

References

Anber, U., Gentine, P., Wang, S., & Sobel, A. H. (2015). Fog and rain in the Amazon. *Proceedings of the National Academy of Sciences*, *112*(37), 11473–11477. https://doi.org/10.1073/pnas.1505077112

Bailly-Comte, V., Jourde, H., Roesch, A., Pistre, S., & Batiot-Guilhe, C. (2008). Time series analyses for karst/river interactions assessment: Case of the Coulazou river (southern France). *Journal of hydrology*, *349*(1–2), 98–114. https://doi.org/10.1016/j.jhydrol.2007.10.028

Berg, A., & Sheffield, J. (2018). Soil moisture–evapotranspiration coupling in CMIP5 models: Relationship with simulated climate and projections. *Journal of Climate*, *31*(12), 4865–4878. https://doi.org/10.1175/jcli-d-17-0757.1

Bonan, G. B. (1996). *Land surface model (LSM version 1.0) for ecological, hydrological, and atmospheric studies: Technical description and users guide. Technical note* (No. PB-97-131494/XAB; NCAR/TN-417-STR). Boulder, CO, United States: National Center for Atmospheric Research. Climate and Global Dynamics Div.

Bourke, P. (1998). Generating noise with different power spectra laws.

Brodzik, M. J., Billingsley, B., Haran, T., Raup, B., & Savoie, M. H. (2012). EASE-Grid 2.0: Incremental but significant improvements for Earth-gridded data sets. *ISPRS International Journal of Geo-Information*, *1*(1), 32–45. https://doi.org/10.3390/ijgi1010032

Chan, S. (2016). Enhanced level 3 passive soil moisture product specification document. Pasadena, CA, USA: Jet propulsion laboratory, California Institute of Technology.

Chan, S. K., Bindlish, R., O'Neill, P., Jackson, T., Njoku, E., Dunbar, S., et al. (2018). Development and assessment of the SMAP enhanced passive soil moisture product. *Remote Sensing of Environment*, *204*, 931–941. https://doi.org/10.1016/j.rse.2017.08.025

Chan, S. K., Bindlish, R., O'Neill, P. E., Njoku, E., Jackson, T., Colliander, A., et al. (2016). Assessment of the SMAP passive soil moisture product. *IEEE Transactions on Geoscience and Remote Sensing*, *54*(8), 4994–5007. https://doi.org/10.1109/tgrs.2016.2561938

Chen, F., Crow, W. T., Bindlish, R., Colliander, A., Burgin, M. S., Asanuma, J., & Aida, K. (2018). Global-scale evaluation of SMAP, SMOS and ASCAT soil moisture products using triple collocation. *Remote Sensing of Environment*, *214*, 1–13. https://doi.org/10.1016/j.rse.2018.05.008

Colliander, A., Jackson, T. J., Bindlish, R., Chan, S., Das, N., Kim, S. B., et al. (2017). Validation of SMAP surface soil moisture products with core validation sites. *Remote Sensing of Environment*, *191*, 215–231. https://doi.org/10.1016/j.rse.2017.01.021

Colliander, A., Reichle, R., Crow, W., Cosh, M. H., Chen, F., Chan, S. K., et al. (2021). Validation of soil moisture data products from the NASA SMAP mission. *IEEE Journal of Selected Topics in Applied Earth Observations and Remote Sensing*.

Delworth, T. L., & Manabe, S. (1988). The influence of potential evaporation on the variabilities of simulated soil wetness and climate. *Journal of Climate*, *1*(5), 523–547. https://doi.org/10.1175/1520-0442(1988)001<0523:tiopeo>2.0.co;2

Dirmeyer, P. A., Jin, Y., Singh, B., & Yan, X. (2013). Trends in land–atmosphere interactions from CMIP5 simulations. *Journal of Hydrometeorology*, *14*(3), 829–849. https://doi.org/10.1175/jhm-d-12-0107.1

Dorigo, W. A., Wagner, W., Hohensinn, R., Hahn, S., Paulik, C., Xaver, A., et al. (2011). The International Soil Moisture Network: A data hosting facility for global in situ soil moisture measurements. *Hydrology and Earth System Sciences*, *15*(5), 1675–1698. https://doi.org/10.5194/hess-15-1675-2011

Dorigo, W. A., Xaver, A., Vreugdenhil, M., Gruber, A., Hegyiová, A., Sanchis-Dufau, A. D., et al. (2013). Global automated quality control of in situ soil moisture data from the International Soil Moisture Network. *Vadose Zone Journal*, *12*(3), 1–21. https://doi.org/10.2136/vzj2012.0097

Entekhabi, D., Njoku, E. G., O'Neill, P. E., Kellogg, K. H., Crow, W. T., Edelstein, W. N., et al. (2010). The soil moisture active passive (SMAP) mission. *Proceedings of the IEEE*, *98*(5), 704–716. https://doi.org/10.1109/jproc.2010.2043918

Entekhabi, D., Yueh, S., & De Lannoy, G. (2014). SMAP handbook.

Famiglietti, J. S., & Rodell, M. (2013). Water in the balance. *Science*, *340*(6138), 1300–1301. https://doi.org/10.1126/science.1236460

Feng, H., & Liu, Y. (2015). Combined effects of precipitation and air temperature on soil moisture in different land covers in a humid basin. *Journal of Hydrology*, *531*, 1129–1140. https://doi.org/10.1016/j.jhydrol.2015.11.016

Ford, T. W., Rapp, A. D., Quiring, S. M., & Blake, J. (2015). Soil moisture–precipitation coupling: Observations from the Oklahoma mesonet and underlying physical mechanisms. *Hydrology and Earth System Sciences*, *19*(8), 3617–3631. https://doi.org/10.5194/hess-19-3617-2015

Ghannam, K., Nakai, T., Paschalis, A., Oishi, C. A., Kotani, A., Igarashi, Y., et al. (2016). Persistence and memory timescales in root-zone soil moisture dynamics. *Water Resources Research*, *52*(2), 1427–1445. https://doi.org/10.1002/2015wr017983

Green, J. K., Seneviratne, S. I., Berg, A. M., Findell, K. L., Hagemann, S., Lawrence, D. M., & Gentine, P. (2019). Large influence of soil moisture on long-term terrestrial carbon uptake. *Nature*, *565*(7740), 476. https://doi.org/10.1038/s41586-018-0848-x

Guo, Z., Dirmeyer, P. A., Hu, Z. Z., Gao, X., & Zhao, M. (2006). Evaluation of the second global soil wetness project soil moisture simulations: 2. Sensitivity to external meteorological forcing. *Journal of Geophysical Research*, *111*(D22). https://doi.org/10.1029/2006jd007845

Haykin, S., & Van Veen, B. (2007). *Signals and systems*. John Wiley and Sons.

Hersbach, H., Bell, B., Berrisford, P., Biavati, G., Horányi, A., Muñoz Sabater, J., & Thépaut, J.-N. (2018). ERA5 hourly data on single levels from 1979 to present. Copernicus Climate Change Service (C3S) Climate Data Store (CDS). https://doi.org/10.24381/cds.adbb2d47

Jiao, D., Xu, N., Yang, F., & Xu, K. (2021). Evaluation of spatial-temporal variation performance of ERA5 precipitation data in China. *Scientific Reports*, *11*(1), 1–13. https://doi.org/10.1038/s41598-021-97432-y

Katul, G. G., Porporato, A., Daly, E., Oishi, A. C., Kim, H. S., Stoy, P. C., et al. (2007). On the spectrum of soil moisture from hourly to interannual scales. *Water Resources Research*, *43*(5). https://doi.org/10.1029/2006wr005356

Koster, R. D., Dirmeyer, P. A., Guo, Z., Bonan, G., Chan, E., Cox, P., et al. (2004). Regions of strong coupling between soil moisture and precipitation. *Science*, *305*(5687), 1138–1140. https://doi.org/10.1126/science.1100217

Koster, R. D., Guo, Z., Yang, R., Dirmeyer, P. A., Mitchell, K., & Puma, M. J. (2009). On the nature of soil moisture in land surface models. *Journal of Climate*, *22*(16), 4322–4335. https://doi.org/10.1175/2009jcli2832.1

Levine, P. A., Randerson, J. T., Swenson, S. C., & Lawrence, D. M. (2016). Evaluating the strength of the land–atmosphere moisture feedback in Earth system models using satellite observations. *Hydrology and Earth System Sciences*, *20*(12), 4837–4856. https://doi.org/10.5194/hess-20-4837-2016

Mandelbrot, B. B. (1982). *The fractal geometry of nature* (Vol. 2). New York: WH Freeman.

Martens, B., Schumacher, D. L., Wouters, H., Muñoz-Sabater, J., Verhoest, N. E., & Miralles, D. G. (2020). Evaluating the land-surface energy partitioning in ERA5. *Geoscientific Model Development*, *13*(9), 4159–4181. https://doi.org/10.5194/gmd-13-4159-2020

McCabe, G. J., & Wolock, D. M. (2013). Temporal and spatial variability of the global water balance. *Climatic Change*, *120*(1), 375–387. https://doi.org/10.1007/s10584-013-0798-0

McColl, K. A., Wang, W., Peng, B., Akbar, R., Short Gianotti, D. J., Lu, H., et al. (2017). Global characterization of surface soil moisture drydowns. *Geophysical Research Letters*, *44*(8), 3682–3690. https://doi.org/10.1002/2017gl072819

Nakai, T., Katul, G. G., Kotani, A., Igarashi, Y., Ohta, T., Suzuki, M., & Kumagai, T. O. (2014). Radiative and precipitation controls on root zone soil moisture spectra. *Geophysical Research Letters*, *41*(21), 7546–7554. https://doi.org/10.1002/2014gl061745

O'Neill, P., Bindlish, R., Chan, S., Njoku, E., & Jackson, T. (2018). Algorithm theoretical basis document. In *Level 2 and 3 soil moisture (passive) data products*.

O'Neill, P. E., Chan, S., Njoku, E. G., Jackson, T., Bindlish, R., & Chaubell, J. (2020). *SMAP L3 radiometer global daily 36 km EASE-grid soil moisture, version 7*. Boulder, Colorado USA: NASA National Snow and Ice Data Center Distributed Active Archive Center. https://doi.org/10.5067/HH4SZ2PXSP6A

Parker, W. S. (2016). Reanalyses and observations: What's the difference? *Bulletin of the American Meteorological Society*, *97*(9), 1565–1572. https://doi.org/10.1175/bams-d-14-00226.1

Pelos, A., Terribile, F., D'Urso, G., & Chirico, G. B. (2020). Comparison of ERA5-land and UERRA MESCAN-SURFEX reanalysis data with spatially interpolated weather observations for the regional assessment of reference evapotranspiration. *Water*, *12*(6), 1669.

Pelosi, A., & Chirico, G. B. (2021). Regional assessment of daily reference evapotranspiration: Can ground observations be replaced by blending ERA5-Land meteorological reanalysis and CM-SAF satellite-based radiation data? *Agricultural Water Management*, *258*, 107169. https://doi.org/10.1016/j.agwat.2021.107169

Phillips, C. L., Parr, J. M., & Riskin, E. A. (2003). *Signals, systems, and transforms* (pp. 209). Prentice Hall.

Riegger, J., & Tourian, M. J. (2014). Characterization of runoff-storage relationships by satellite gravimetry and remote sensing. *Water Resources Research*, *50*(4), 3444–3466. https://doi.org/10.1002/2013wr013847

Rivoire, P., Martius, O., & Naveau, P. (2021). A comparison of moderate and extreme ERA-5 daily precipitation with two observational data sets. *Earth and Space Science*, *8*(4), e2020EA001633. https://doi.org/10.1029/2020ea001633

Salvucci, G. D., & Entekhabi, D. (1994). Equivalent steady soil moisture profile and the time compression approximation in water balance modeling. *Water Resources Research*, *30*(10), 2737–2749. https://doi.org/10.1029/94wr00948

Santanello, J. A., Jr., Dirmeyer, P. A., Ferguson, C. R., Findell, K. L., Tawfik, A. B., Berg, A., et al. (2018). Land–atmosphere interactions: The LoCo perspective. *Bulletin of the American Meteorological Society*, *99*(6), 1253–1272. https://doi.org/10.1175/bams-d-17-0001.1

Sehler, R., Li, J., Reager, J. T., & Ye, H. (2019). Investigating relationship between soil moisture and precipitation globally using remote sensing observations. *Journal of Contemporary Water Research and Education*, *168*(1), 106–118. https://doi.org/10.1111/j.1936-704x.2019.03324.x

Seneviratne, S. I., Corti, T., Davin, E. L., Hirschi, M., Jaeger, E. B., Lehner, I., et al. (2010). Investigating soil moisture–climate interactions in a changing climate: A review. *Earth-Science Reviews*, *99*(3–4), 125–161. https://doi.org/10.1016/j.earscirev.2010.02.004

Seneviratne, S. I., Koster, R. D., Guo, Z., Dirmeyer, P. A., Kowalczyk, E., Lawrence, D., et al. (2006). Soil moisture memory in AGCM simulations: Analysis of global land–atmosphere coupling experiment (GLACE) data. *Journal of Hydrometeorology*, *7*(5), 1090–1112. https://doi.org/10.1175/jhm533.1

Su, C. H., Ryu, D., Crow, W. T., & Western, A. W. (2014). Stand-alone error characterisation of microwave satellite soil moisture using a Fourier method. *Remote sensing of environment*, *154*, 115–126. https://doi.org/10.1016/j.rse.2014.08.014

Suni, T., Guenther, A., Hansson, H. C., Kulmala, M., Andreae, M. O., Arneth, A., et al. (2015). The significance of land-atmosphere interactions in the Earth system—iLEAPS achievements and perspectives. *Anthropocene*, *12*, 69–84. https://doi.org/10.1016/j.ancene.2015.12.001

Tarek, M., Brissette, F. P., & Arsenault, R. (2020). Evaluation of the ERA5 reanalysis as a potential reference dataset for hydrological modelling over North America. *Hydrology and Earth System Sciences*, *24*(5), 2527–2544.

Taylor, K. E., Stouffer, R. J., & Meehl, G. A. (2012). An overview of CMIP5 and the experiment design. *Bulletin of the American Meteorological Society*, *93*(4), 485–498. https://doi.org/10.1175/bams-d-11-00094.1

Thomson, R. E., & Emery, W. J. (2014). *Data analysis methods in physical oceanography*. Newnes.

Wang, Y., Zhang, Y., Yu, X., Jia, G., Liu, Z., Sun, L., et al. (2021). Grassland soil moisture fluctuation and its relationship with evapotranspiration. *Ecological Indicators*, *131*, 108196. https://doi.org/10.1016/j.ecolind.2021.108196

Wilks, D. S. (2011). *Statistical methods in the atmospheric sciences* (Vol. 100). Academic Press.

Wrona, E., Rowlandson, T. L., Nambiar, M., Berg, A. A., Colliander, A., & Marsh, P. (2017). Validation of the soil moisture active passive (SMAP) satellite soil moisture retrieval in an arctic tundra environment. *Geophysical Research Letters*, *44*(9), 4152–4158. https://doi.org/10.1002/2017gl072946

Wu, W., Geller, M. A., & Dickinson, R. E. (2002). The response of soil moisture to long-term variability of precipitation. *Journal of Hydrometeorology*, *3*(5), 604–613. https://doi.org/10.1175/1525-7541(2002)003<0604:trosmt>2.0.co;2

Xi, X., Gentine, P., Zhuang, Q., & Kim, S. (2022). Evaluating the variability of surface soil moisture simulated within CMIP5 using SMAP data. *Journal of Geophysical Research: Atmospheres*, *127*(5), e2021JD035363. https://doi.org/10.1029/2021jd035363

Yao, P., & Lu, H. (2020). *A long term global daily soil moisture dataset derived from AMSR-E and AMSR2 (2002-2020)*. National Tibetan Plateau Data Center. https://doi.org/10.11888/Soil.tpdc.270960

Yuan, S., Quiring, S. M., & Leasor, Z. T. (2021). Historical changes in surface soil moisture over the contiguous United States: An assessment of CMIP6. *Geophysical Research Letters*, *48*(1), e2020GL089991. https://doi.org/10.1029/2020gl089991

Zhou, Y., Dong, X., Chen, H., Cao, L., Shao, Q., Sun, S., et al. (2020). Sub-seasonal variability of surface soil moisture over eastern China. *Climate Dynamics*, *55*(11), 3527–3541. https://doi.org/10.1007/s00382-020-05464-3

References From the Supporting Information

Gilman, D. L., Fuglister, F. J., & Mitchell, J. M., Jr. (1963). On the power spectrum of "red noise". *Journal of the Atmospheric Sciences*, *20*(2), 182–184.

Partington, J. R. (2004). *Linear operators and linear systems: An analytical approach to control theory* (No. 60). Cambridge University Press.

Steele, J. H. (1985). A comparison of terrestrial and marine ecological systems. *Nature*, *313*(6001), 355–358.

Vasseur, D. A., & Yodzis, P. (2004). The color of environmental noise. *Ecology*, *85*(4), 1146–1152.